JOURNAL OF MATERIALS SCIENCE **36** (2001) 2547–2555

Corrosion behaviour of some stainless steel alloys in molten alkali carbonates (I)

S. A. SALIH, A. N. EL-MASRI, A. M. BARAKA
Chemistry Department, Faculty of Science, Cairo University, Giza, Egypt
E-mail: said@chem-sci.cairo.eun.eg

In the present work it is aimed to study the corrosion behaviour of two types of stainless steel alloys (one ferritic and two austenitic) in molten Li_2CO_3- Na_2CO_3- K_2CO_3 mixture. This mixture is of interest in corrosion studies because of its low melting point (397°C) and good electrical properties. In this investigation the following techniques of measurements are used: (i) open circuit-potential, (ii) galvanic current, (iii) impedance, (iv) atomic absorption spectroscopy for the determination of the amount of metals dissolved in the melt (v) corrosion tests, carried out on the oxide scales formed during the oxidation of stainless steel alloys in carbonate melt. In this melt the electrode Ag/AgCl was used as a reference electrode. In molten carbonates, the oxide ions originate by self-dissociation according to the equilibrium $CO_3^{2-} \leftrightarrow CO_2 + O^{2-}$. The oxide ions, O^{2-}, and carbonate ions, CO_3^{2-}, play an important role in the oxidation process of these alloys and their passivation in the carbonate melt. As previously mentioned in references it can be assumed that the oxide scales formed on the alloy surface consist mainly of $LiCrO_2$ and $LiFeO_2$. The cathodic path of the corrosion process may be the reduction of CO_2 and/or CO_3^{2-}. The resistance of alloys against corrosion in melt increases with the increase of temperature. This may be due to the increase of concentration of O^{2-} and CO_2, enhancing both the anodic and cathodic reactions. The activation energy was calculated and found to be 91.496, 23.412 and 37.956 kJ/mol for the alloys 1, 2 and 3 respectively. The above mentioned techniques of measurements showed that the oxide scales of the austenitic stainless steel alloys (2, 3) are more passive and protective than of ferritic stainless steel alloy (1). This means that the resistance against corrosion, in the carbonate melts, of austenitic stainless steel alloys is higher than that of ferritic one.

1. Introduction

Interest in use of fused salts in industrial processes is continually increasing and these media are gradually becoming accepted as a normal field of chemical engineering.

Molten salts in particular alkali metal halides, nitrates, sulphates and carbonates possess properties which make them desirable in the development of efficient methods of materials processing and energy production.

Molten alkali carbonates, in view of fuel cell application, have drawn the interest of scientists for thirty years. More recently, these media appeared to have possible developments for recovery of hydrogen, methane or other hydrocarbons from natural biocompounds. In these organic processes, some potentially corrosive compounds such as oxygen or water are formed.

Material degradation owing to corrosion is an important issue virtually all energy producing systems, including the advanced molten carbonate fuel cells now under development. Current collectors and other metallic components of the fuel cell may be rapidly degraded at high temperatures if molten salt contacts the surface. This form of attack is thought to be due to "fluxing" wherein the normally protective oxide scale on an alloy destroyed by dissolution-precipitation mechanism.

Reaction between alloys and molten carbonates are technologically important in view of the long term stability and compatibility of materials associated with molten carbonate fuel cells.

The molten carbonate fuel cells has been continues to be under intensive investigation and development. The corrosion behaviour of stainless steel and other alloys were the subjected to study in molten alkali carbonate by many investigators [1–13]. Most of these studies were carried out under the conditions of operation of molten carbonate fuel cells.

In this article it is aimed to study the corrosion behaviour of two types of stainless steel alloys in ternary Li_2CO_3- Na_2CO_3- K_2CO_3 molten mixture. This mixture is of interest in corrosion studies because of its low melting point (397°C) and good electrical properties. In this investigation the following techniques of measurements are used: (i) open circuit-potential, (ii) galvanic current, (iii) impedance, (iv) atomic absorption spectroscopy for the determination of the amount of metals

dissolved in the melt (v) corrosion tests, carried out on the oxide scales formed during the oxidation of stainless steel alloys in carbonate melt.

2. Experimental

In the present investigation of the corrosion behaviour of one ferritic (15.05% Cr) and two austenitic stainless steel alloys (17.9% Cr, 7.08% Ni and 20.45% Cr, 8.3% Ni) was studied in molten Li_2CO_3- Na_2CO_3- K_2CO_3 mixture (43.5 : 31.5 : 25 mole % respectively). The calculated quantities of carbonates were mixed together in a special container and placed in an electrically heated furnace and melted at 550°C. The last trace of water removed by bubbling through the melt, pure dry CO_2 gas for a period of 2 hours. The mixture thus prepared was left to cool in a dry atmosphere and solidified mass was quickly crushed and kept in a closed desiccator till required. In each experiment 50.0 g of the ternary mixture was used.

The electrochemical cell used in this study consisted of an outer cylindrical closed end alumina crucible (500 ml capacity) in which a smaller Pyrex glass tube (100 ml capacity) was placed. The latter contained the electrolyte and electrodes. The cell was rendered gas tight by means of O-ring seal between the outer alumina crucible and a stainless steel header from which the electrodes tubes were fixed.

The cell and its contents was heated to the required temperature throughout the period of the experimental in an electric vertical tube furnace. The temperature of the furnace was regulated by means of a veriable transformer and followed by means of a Ni/Ni-Cr thermocouple and a temperature indicator. In all experiments, the desired temperature was precisely adjusted in a limit of ±2°C. The thermocouple was contained in a special tube to separate it from the melt.

Stainless steel electrodes were cut from ferritic (alloy no.1) and austenitic (alloy no. 2, 3) stainless steel sheets of thickness 1 mm. These electrodes were of dimensions 1×1 cm^2 with a side arm of about 20 cm long and 0.2 cm width, used for electrical connection. This arm is coated by a pyrex glass tube of suitable diameter which fitted to the arm at the upper end by an adhesive. In each experiment a new electrode was used. Just before of its immersion in the melt, the electrode was abraded with emery papers of different grades and degreased with ether.

In this melt the electrode Ag/AgCl was used as a reference electrode. The reversibility of this electrode and its stability to function as a reference one was established by many authors [14–17].

The potential of working elctrode, relative to the reference electrode, was measured on a D.C. Microvoltmeter (type TM8 Level Electronic LTD, England). The galvanic current in microamperes was measured on digitalmultimeter (Model 1008, Kyoritsu Electrical Instruments work, LTD Japan). The impedance measurements are carried out using Impedance Measurements System (1M6 Zahner Electrik, Meßtechnik, Germany). The atomic adsorption measurements are carried out using flame-atomic absorption spectrophotometer (Perkin-Elmer Apparatus Model 23, Germany).

3. Results and discussion

3.1. Open circuit potential measurements (OCP)

The variation of the corrosion potential, E_{corr}, of the stainless steel alloys (no. 1, 2, 3), under open circuit conditions in molten Li_2CO_3- Na_2CO_3- K_2CO_3 mixture, was followed as a function of time till steady state values were established. The curves of Fig. 1a–c show, respectively, the behaviour of the stainless steel alloys at temperatures 475, 500, 525, and 550°C. It could be seen that the corrosion potential of the alloys firstly shifts in the positive direction reaching maximum. After this the potential starts to move in the active direction till attaining its steady state.

The results of open circuit potential measurements for the three stainless steel alloys are depicted in Fig. 2a–c as E_{corr} versus logarithm of time at different temperatures. It is clear from these plots that, before attaining the steady state potential, the obtained lines contain two segments. The slopes of these segments are determined, k_f, k_{-f} which are taken as a measure of the rate of the formation and dissolution processes of

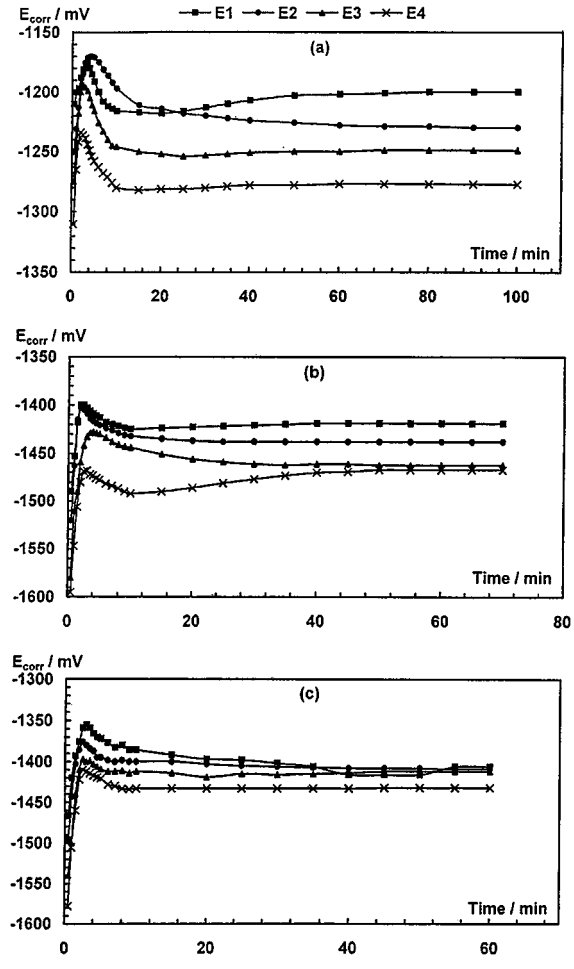

Figure 1 Variation of corrosion potential, E_{corr} of the stainless steel alloys with time in pure carbonate melt at different temperatures. E1, 475°C.E2, 500°C.E3, 525°C.E4, 550°C. (a) alloy 1. (b) alloy 2. (c) alloy 3.

TABLE I Data of the open circuit potential measurements for the stainless steel alloys at different temperatures

Alloy	Temp. °C	E_{imm} (mV)	E_s (mV)	$E_s - E_{imm}$ (mV)	t_s min	k_f mV decade^{-1}	k_{-f} mV decade^{-1}
st.st-1	475	−1210	−1200	10	80	33.892	107.92
	500	−1250	−1230	20	90	86.416	87.782
	525	−1275	−1249	26	40	124.83	108.49
	550	−1310	−1277	33	15	129.75	74.867
st.st-2	475	−1490	−1419	71	40	151.65	43.356
	500	−1520	−1438	82	25	202.59	42.164
	525	−1580	−1462	118	30	195.13	55.974
	550	−1595	−1467	128	50	223.74	45.04
st.st-3	475	−1466	−1406	60	35	152.5	64.234
	500	−1489	−1408	81	40	167.92	67.788
	525	−1540	−1412	128	45	219.36	39.131
	550	−1578	−1432	146	45	256.55	36.286

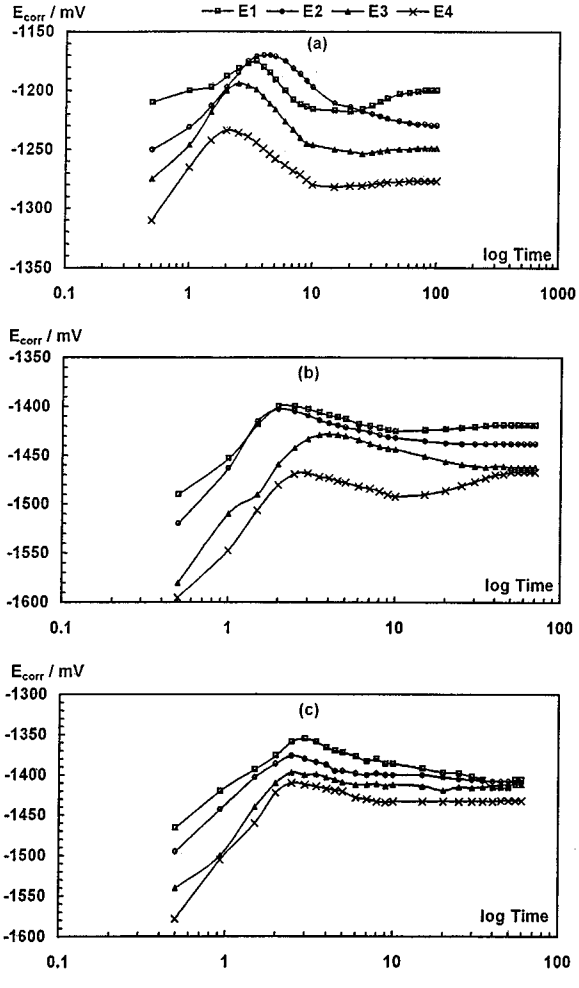

Figure 2 Variation of corrosion potential, E_{corr}, of the stainless steel alloys with log (time) in pure carbonate melt at different temperatures. $E1$, 475°C. $E2$, 500°C. $E3$, 525°C. $E4$, 550°C, (a), alloy 1, (b) alloy 2, (c) alloy 3.

the oxide scale, respectively. The value of these rates are different and depend on the type of stainless steel alloy and temperature of the melt. Table I includes the values of E_{imm} (potential at the moment of immersion in melt), E_s (steady state potential), (E_s- E_{imm}), k_f and k_{-f} for the three stainless steel alloys at different temperatures.

Fig. 3a and b represent, respectively, the variation of (E_s- E_{imm}), k_f and k_{-f} as a function of chromium

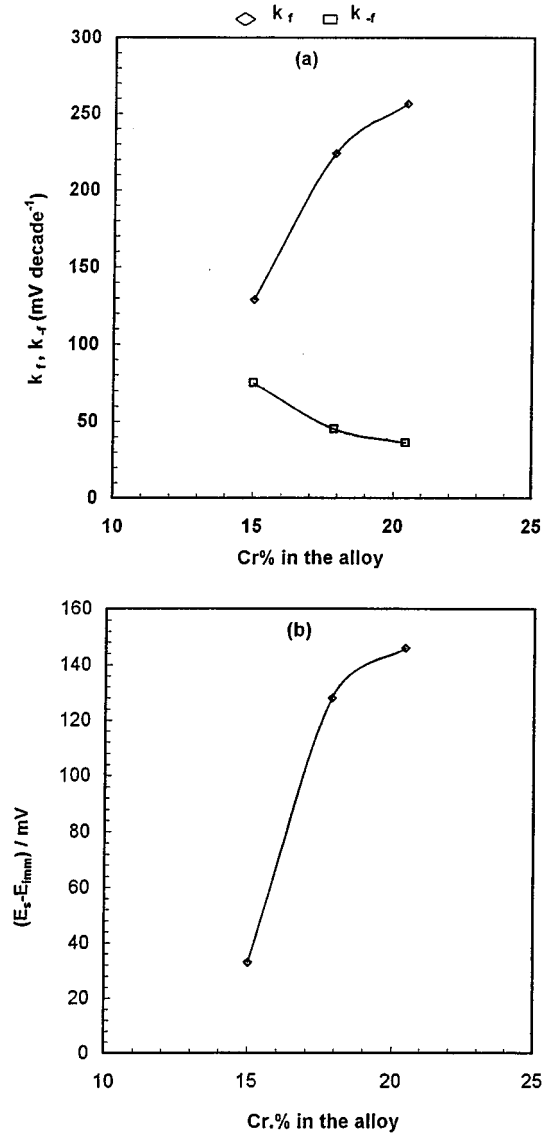

Figure 3 (a): k_f, k_{-f} vs. Cr (wt%) in the alloy at 550°C. (b): ($E_s - E_{imm}$) vs. Cr (wt%) in the alloy 550°C.

content of the stainless steel alloys at a temperature of 550°C.

Fig. 4a and b represent, respectively, the variation of k_f, k_{-f} and (E_s- E_{imm}), as a function of iron content of the stainless steel alloys at a temperature of 550°C.

Fig. 5a and b represent the variation of the amount of Cr and Fe (wt %) dissolved in melt as a function of Cr and Fe contents of the stainless steel alloys, respectively, at a temperature of 550°C.

In molten carbonate the oxide ions originate by self-dissociation according to the equilibrium:

$$CO_3^{2-} \leftrightarrow CO_2 + O^{2-} \quad (1)$$

this reaction is responsible for the presence of oxide ions in the carbonate melt. In Lux–Flood acid–base properties, CO_2 is the acid and O^{2-} the base. It can be assumed that the oxide ions, O^{2-}, and carbonate ions, CO_3^{2-}, play the important role in the oxidation process of the stainless steel alloys in the carbonate melt. Thus the reactions leading to the oxidation of different metals in the alloys may be represented by the

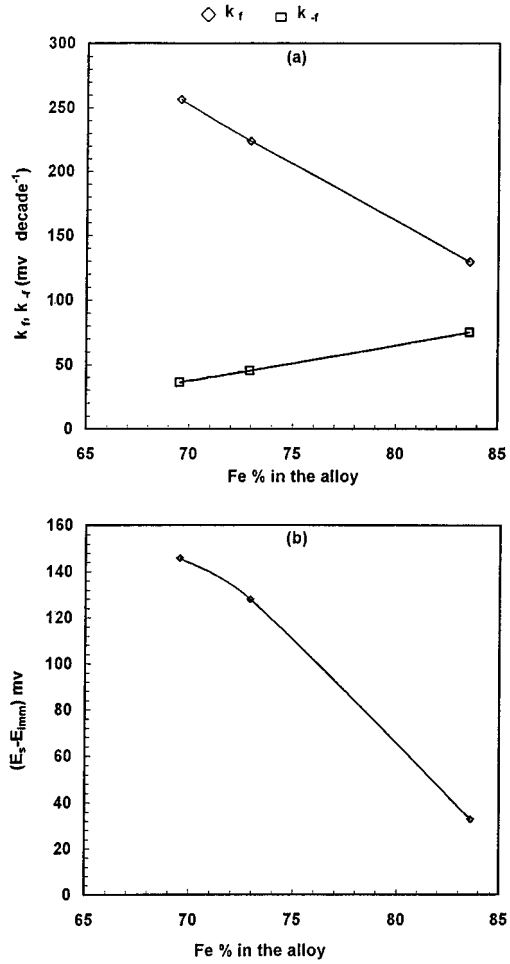

Figure 4 (a): k_f, k_{-f} vs. Fe % in the alloy at 550°C. (b): $(E_s - E_{imm})$ vs. Fe % in the alloy at 550°C.

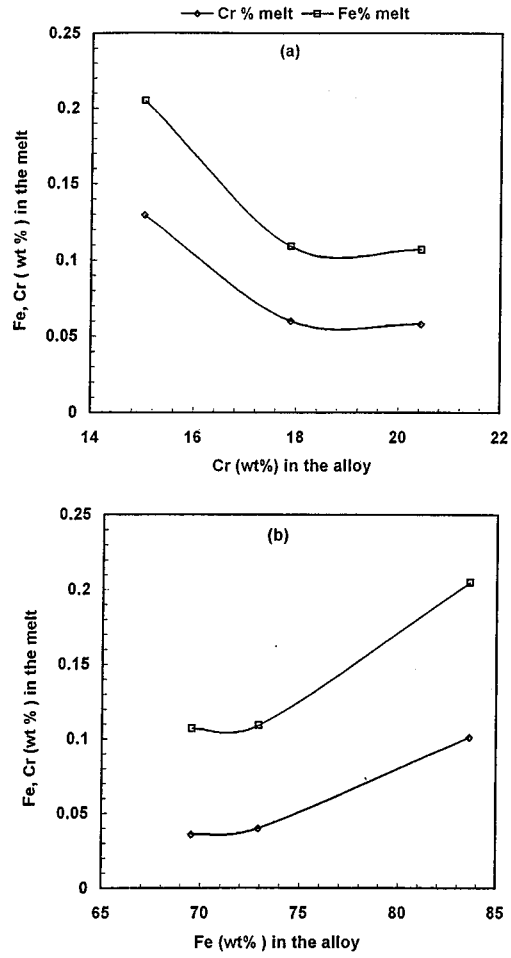

Figure 5 (a): Fe, Cr (wt %) in the melt vs. Cr (wt %) in the alloy at 550°C. (b): Fe, Cr (wt %) in the melt vs. Fe (wt %) in the alloy at 550°C.

following equations:

$$M + n/2\, O^{2-} \leftrightarrow MO_{n/2} - ne \quad (2)$$

and/or

$$M + n/2\, CO_3^{2-} \leftrightarrow MO_{n/2} + n/2\, CO_2 + ne \quad (3)$$

in the case of carbonate melts and the undertest stainless steel alloys, it can be proposed, as in the previous works of Vossen *et al*. [18, 19], that the oxidation and passivation of the alloys may proceed according to the following paths:

$$Cr + Li^+ + 2CO_3^{2-} \rightarrow LiCrO_2 + 2CO_2 + 3e \quad (4)$$

$$Fe + CO_3^{2-} \rightarrow FeO_{ss} + CO_2 + 2e \quad (5)$$

$$Fe + Li^+ + 2CO_3^{2-} \rightarrow LiFeO_{2ss} + 2CO_2 + 3e \quad (6)$$

A cubic solid solution (ss) FeO and $LiFeO_2$ is formed. However, FeO is stable only above 570°C, therefore FeO may decompose to Fe_3O_4 and, apparently Fe_2O_3 at temperatures lower than 570°C as:

$$3FeO + O^{2-} = Fe_3O_4 + 2e \quad (7)$$

$$2Fe_3O_4 + O^{2-} = 3Fe_2O_3 + 2e \quad (8)$$

The possible cathodic reactions in the molten carbonate may be [18–20].

$$3CO_2 + 4e \rightarrow C + 2CO_3^{2-} \quad (9)$$

$$CO_3^{2-} + 4e \rightarrow C + 3O^{2-} \quad (10)$$

and/or

$$2CO_2 + 2e \rightarrow CO + CO_3^{2-} \quad (11)$$

$$CO_3^{2-} + 2e \rightarrow CO + 2O^{2-} \quad (12)$$

According to the postulate of the electrochemical theory, the anodic process may be metal dissolution and/or anodic barrier layer formation. Barrier layer may be formed by dissolution-precipitation mechanism and/or solid state mechanism. For many passive metals, it was found that the thickness of oxide scale, x, varies linearly with the electrode potential either under polarization [21] or under open circuit conditions [22–24], i.e $dE_{corr/dx} = \text{const}$. The constant is actually the electric field strength, H, i.e. $E_{corr} \alpha x$ and the equation relating E_{corr} and time, t, can be written as:

$$E_{corr} = k_1 + k_2 \log(t + t^\circ)^- \quad (13)$$

where k_1, k_2 and t° are constants. The constant k_2 is taken as a measure for the rate of oxide scale thickening

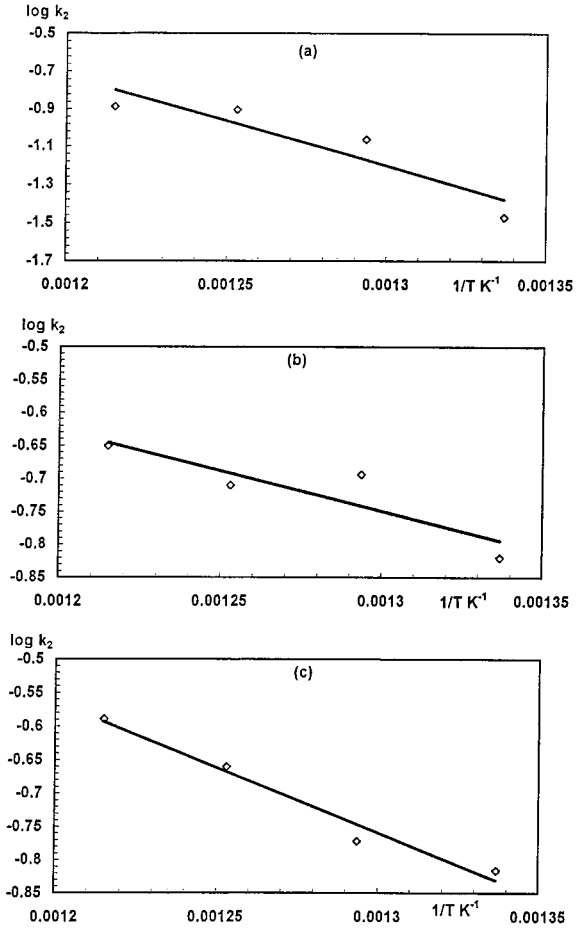

Figure 6 Variation of log k_2 with the reciprocal of the absolute temperature for stainless steel alloys in the pure carbonate melt. (a) alloy 1. (b) alloy 2. (c) alloy 3.

per decade of time and has the meaning of k_f (previously mentioned).

In the early stages of oxidation the increase of corrosion potential in the positive direction is attributed to covering the metal surface with a barrier film [25]. The experimental results show that this film grows at a rate, magnitude of which depends on the temperature of the metal and type of alloy. The value of k_2 increases with increase of temperature from 475°C to 550°C. Also, the value of k_2 for stainless steel alloys 2 and 3 are higher than those for stainless steel alloys 1.

Fig. 6a–c represent the Arrhenius plots of log k_2 versus 1/T for the stainless steel alloys, respectively. The calculated values of activation energy are: 91.496 kJ/mol for alloy 1, 23.412 kJ/mol for alloy 2 and 37.956 kJ/mol for alloy 3. The low values of activation energy for the alloys 2, 3 may signify diffusion-controlled processes occurring in the oxide matrix. On the other hand the higher values of activation energy for alloy (1) may signify activation-controlled processes.

From the results listed in Table I and depicted in Figs 3–5, it is clear that the values of k_f, $E_s - E_{imm}$ are higher for the austenitic stainless steel alloys (2, 3) than those for the ferritic stainless steel alloy (1). For any alloy, these values increases with the increase of temperature. On the other hand the values of k_{-f} and Fe% and Cr% dissolved in the melt are lower for the austenitic stainless steel alloys (2, 3) than those for the ferritic stainless steel alloy (1). For any alloy, the values of k_{-f} decrease with the increase of temperature. Also, it can be concluded that the resistance against corrosion of the undertest stainless steel alloys increases in the order: alloy 1 < alloy2 ≈ alloy3.

Vossen *et al.* [12] studied the corrosion behaviour of five commercially available alloys including stainless steel alloys in molten alkali carbonates and reported the following results. The oxide scale formed on stainless steel alloys is probably a mixture of porous Li-Fe-oxide, Li-Cr-oxide and nickel islands. The corrosion resistance of the alloys increases with the increase of Cr content of the alloy as a result of formation of less porous oxide scale on the metallic surface or formation of (lithium) chromium oxide scale underneath the porous oxide scales. These assumptions are in good agreement with obtained results in the present investigation. The increase of resistance against corrosion of the undertest stainless steel alloys with increase of temperature may be due to increase of the degree of self dissociation of carbonate with the increase of temperature. With increasing temperature the equilibrium $CO_3^{2-} \leftrightarrow CO_2 + O^{2-}$ is shifted to right with the formation of more CO_2 and O^{2-}. The increase of O^{2-} and CO_2 concentration in the melt enhances both, the previously mentioned, anodic and cathodic reactions. This state gives rise to the formation of more thick and protective scales on the electrode surface.

3.2. Galvanic current measurements

This type of measurements was previously used by Benzo and Takeo [26] for studying the oxidation behaviour of stainless steel alloys in alkali nitrate melt. They measured the galvanic current between the stainless steel and Pt electrode, till attaining the steady state. Similarly in this study trials were made to use the galvanic current measurements to study the corrosion behaviour of the undertest alloys in molten carbonate baths. In these measurements the galvanic current between the working electrode and Pt electrode was followed as a function of time, till attaining the steady-state.

Fig. 7 represents the galvanic current-time plots of the three stainless steel alloys (no. 1, 2, 3) immersed in carbonate melt at temperature of 550°C. It is clear

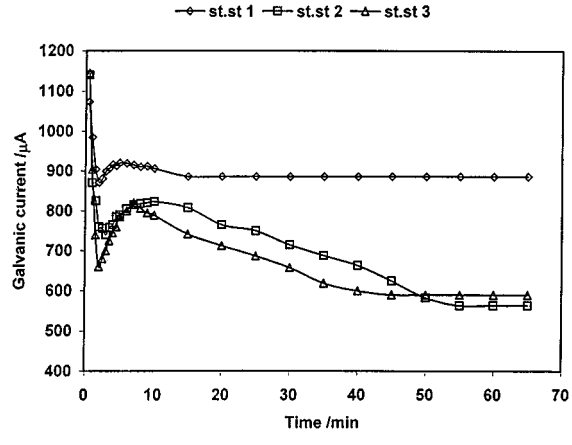

Figure 7 Variation of galvanic current with the time for stainless steel alloys (1, 2, 3) in pure carbonate melt at 550°C.

TABLE II Data of galvanic current measurements for the stainless steel alloys at 550°C

Alloys	Temp. °C	i_{imm} μA	i_s μA	$i_{imm} - i_s$ μA	t_s min
st.st-1	550	1074	886	188	15
st.st-2	550	1140	564	567	50
st.st-3	550	1145	590	555	40

from these plots that, on immersion of the electrode in the carbonate melt, the galvanic current greatly decreases with time reaching minimum values. Afterthis the galvanic current starts to increase reaching maximum and then decrease till steady state values. The values of the galvanic current at the moment of electrode immersion in the melt, i_{imm}, and at the steady state, i_s and the difference $(i_{imm} - i_s)$ are deduced from the plots of Fig. 7 and listed in Table II. If we roughly consider the value of $(i_{imm} - i_s)$ as a measure of thickness and protective properties of oxide scales, the resistance against corrosion for the undertest stainless steel alloys is alloy $1 <$ alloy$2 \approx$ alloy3. These results are in a good agreement with open circuit potential measurements.

3.3. Impedance measurements

In this part the impedance measurements, were used to study the corrosion and oxidation behaviour of the undertest stainleess steel alloys (1, 2, 3) in molten carbonate mixture, at temperature of 550°C. In principle, the method, involves direct measurements of impedance of the electrochemical system in frequency domain from 0.1 to 10^5 Hz. The electrode impedance, Z, and the phase shift (θ) are presented in Bode and Nyquist formats. These experiments are carried out at steady state under open circuit conditions.

Fig. 8a and b represent Bode plots and Fig. 8c represent the Nyquist plot for stainless steel alloys (1, 2, 3). Inspection of the Bode plots indicates that, in most cases, the impedance, Z, remains unchanged in the high frequency region. In the lower frequency region the impedance starts to increase with the decrease of frequency till reaching the end of frequency limit (10^{-1} Hz). The corresponding phase plots have the same trend, except that (θ) has maximum value in the frequency region from 0.5 to 0.2 Hz depending on the type of the stainless steel alloy. The Nyquist plots may be regarded as a plot of a semicircle and not complete semicircle the length of this part increases according to the order: alloy $1 <$ alloy $2 <$ alloy3.

These results and shapes of the plots of Fig. 8a–c are similar to those reported by Walter [27] in his review of impedance plot methods used for corrosion performance analysis of painted metals and also those obtained on iron [28] and nickel [29]. Walter [27] reported that in many cases the equivalent circuit (Randell cell) will not be adequate as a model for the painted metal solution interface. One modification takes into account, diffusion processes within pores in the paint film, which are modelled by the inclusion of a Warburg or pseudo

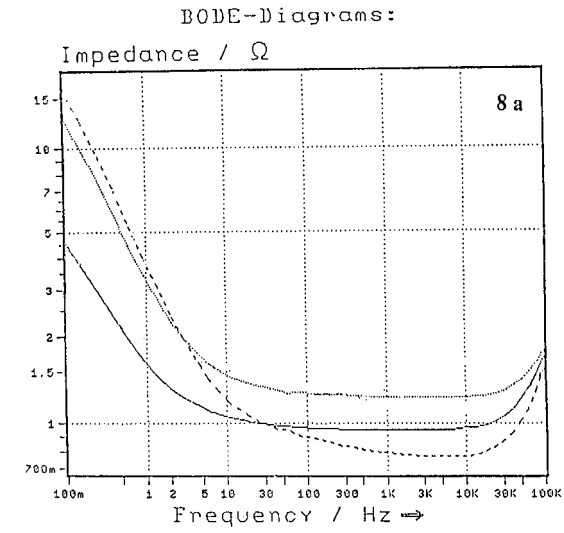

(a)

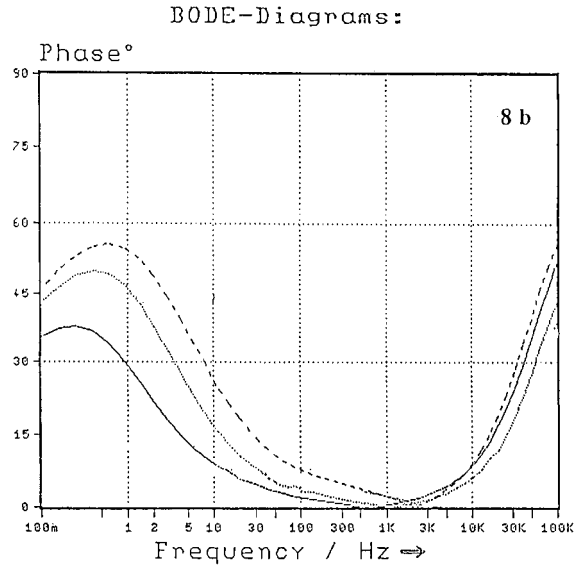

(b)

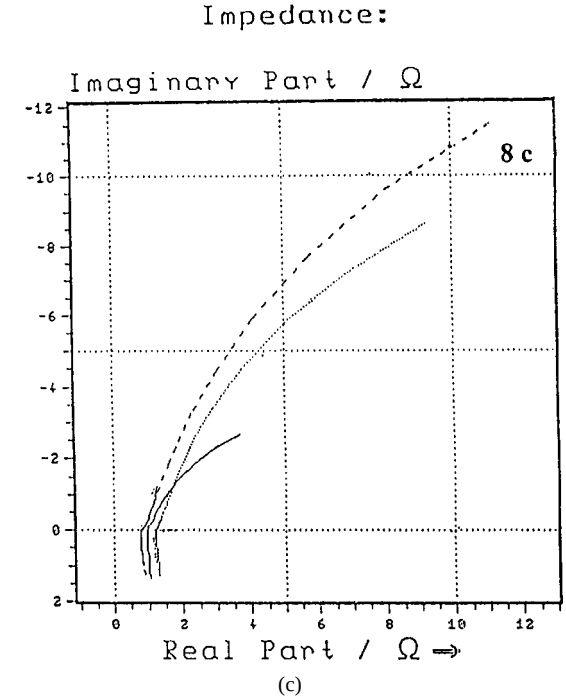

(c)

Figure 8 (a): Bode plot (impedance - frequency) in pure carbonate melt at 500°C. ——alloy 1, ...alloy 2, - - - - - - - - - alloy 3. (b): Bode plot (phase angle - frequency) in pure carbonate melt at 500°C. ——alloy 1, ...alloy 2, - - - - - - - - - alloy 3. (c): Nyquist impedance plot in pure carbonate melt at 500°C. ——alloy 1, ...alloy 2, - - - - - - - alloy 3.

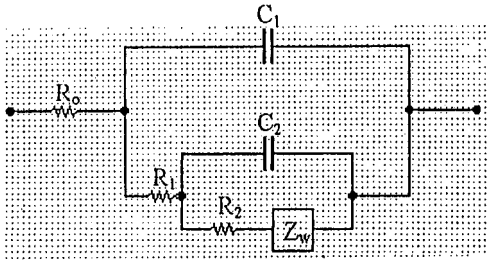

C_1: double layer capacitance.

C_2: capacitance of the oxide layer.

R_o: electrolyte resistance.

R_1: the charge-transfer resistance.

R_2: resistance of oxide layer.

Z_w: Warburg impedance due to diffusion in the oxide layer.

Figure 9 Equivalent electrical circuit, for stainless steel alloys.

impedance, Z_w, placed in series with R_3, where Z_w is defined according to Equation 14.

$$Z_w = \sigma\omega^{-1/2}(1 - j). \tag{14}$$

where σ: Warburg impedance coefficient (ohm$^{1/2}$), ω: angular frequency $= 2\pi f$ (rad s^{-1}), j: imaginary unit $= \sqrt{-1}$.

In our study the equivalent electrical circuit can be shown in Fig. 9. It must be mentioned that in Nyquist plot at $\sigma = 0$ a semicircle can be obtained, but at higher σ values a diffusion tail begins to appear at low frequencies. When values of σ are about equal to R_2, this diffusion tail begins to overlap the semicircle and subtends an angle of 45° to the Z' axis. As σ increases, still further, this overlap becomes increasingly more sever, but the diffusion tail eventually becomes inclined at an angle of 45° to Z' at low frequencies. Finally when σ is significantly greater than R_2 (indicating that the diffusion processes are occurring slower than the metal charge-transfer reaction), the diffusion tail completely distorts the semicircle shape. In Bode plots for the circuit, when there is no diffusion impedance, $\sigma = 0$ and the lower frequency portion of the log Z is a line horizontal to the frequency axis indicating a purely resistive value of modulus Z, equivalent to $(R_0 + R_1 + R_2)$, whilst the phase angle approaches zero. As the value of σ increases, the log Z line at low frequencies is no longer horizontal but curves upward, becoming steeper and approaching a slop of $-\frac{1}{2}$ at high value of σ. The corresponding low frequency portion of the angle plot show values of θ changing from zero towards 45° as σ increases. If the value of σ increases still further, becoming significantly greater than R_2, the slope of $-\frac{1}{2}$ is approached at low frequencies. From the definition of Z_w in Equation 14, the modulus

$$Z = \sqrt{Z'^2 + Z''^2} = \sqrt{2}\sigma\omega^{-1/2}$$

which leads to Equation 15.

$$\log Z = \log\left(\frac{\sigma}{\sqrt{\pi}}\right)^{-1/2} \log f \tag{15}$$

this predicts that a Bode plot of log Z versus solely of Warburg impedance, Z, will be characterized by a lower frequency slope of $-\frac{1}{2}$ and an intercept on the Z_w axis at $F = 1$ Hz of $\sigma/\sqrt{\pi}$.

Estimates of σ can be obtained by finding a region of the Nyquist complex plane plot at low frequencies, where the diffusion tail is inclined at angle of 45° to the axis Z'. Within this region σ can be caluclated from Equation 16 which is obtained from Equation 14.

$$Z'' = \sigma\omega^{-1/2}$$
$$\sigma = \frac{Z''}{\omega^{-1/2}} = Z''\omega^{1/2} \tag{16}$$

calculation of σ values can be made from log Z Bode plots by finding a region at low frequencies where the slope is $-\frac{1}{2}$. By back extrapolation, the value of the Z can be read at frequency of 1 Hz and equated to $\sigma/\sqrt{\pi}$ in order to obtain σ.

The values of: 1) - R_{corr} are calculated from Bode plots at frequency 0.1 Hz by subtracting the value of Z (R_0) at high frequency from the value of Z $(R_0 + R_{corr})$ and from Nyquist plot using the modulus: $Z = \sqrt{Z'^2 + Z''^2} = R''_{corr}$.
2)- σ (Warburg impedance coefficient) are calculated from Bode plots by calculation of Z_w at 1 Hz and by using Equation 15 $(\sigma_1 = Z_w\sqrt{\pi})$, and from Nyquist plots at $f = 0.1$ Hz using equation, $\sigma_2 = Z''\omega^{1/2}$, where $\omega = 2\pi f$ (rad s^{-1}).
3)- the phase angle (θ) at $f = 0.1$ Hz, are deduced from Bode plots. These values are calculated for the stainless steel alloys (1, 2, 3) and listed in Table III. Inspection of these results reveals that: 1)- the values of R_{corr} calculated either from Bode plots or Nyquist plots are near to each other. 2)- the values of R_{corr} increases according the following order st. st alloy 1 < st. st alloy 2 < st. st alloy 3. This may be attributed to the increase of Cr % in the alloys and also to the presence of nickel in the austenitic stainless steel alloys (2, 3). 3)- the values of σ calculated either from Bode plots (at $f = 1$ Hz) or from Nyquist plots ($f = 0.1$ Hz) are near to each other. These values increase according to the above mentioned order. 4)- the phase angle θ at 0.1 Hz increases according to the above mentioned order.

Fig. 10a and b represent respectively the plots of R_{corr} and σ versus Fe% and Cr% of stainless steel alloys.

TABLE III Data of impedance measurements for the stainless steel alloys at 550°C

	Alloy 1	Alloy 2	Alloy 3
R'_{corr} (Ω)	3.62	11.4	15.21
R''_{corr} (Ω)	3.8	11.6	15.4
Z_w (Ω)	1.5	4	5
σ_1 (Ωs$^{1/2}$)	2.66	7.09	8.86
σ_2 (Ωs$^{1/2}$)	2.1	6.7	9.11
$\theta_{(degree)}$	36	44	46

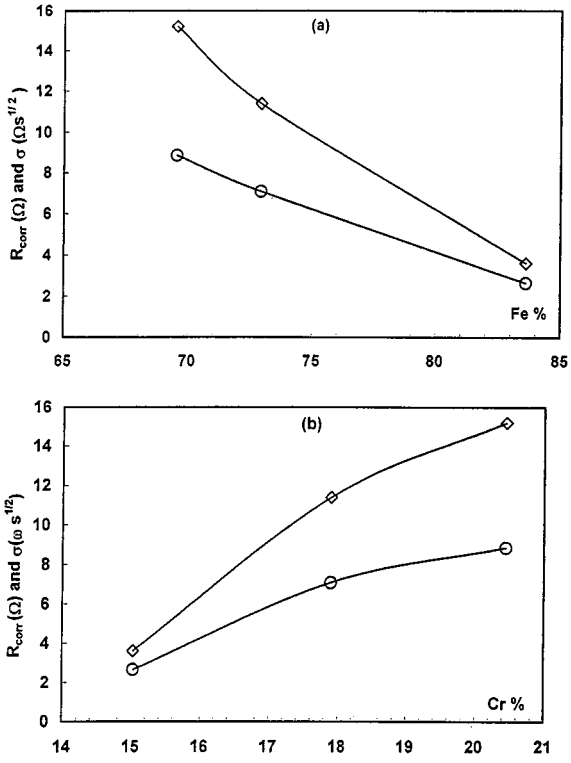

Figure 10 Variation of R_{corr} and σ with Fe% (a) and Cr% (b) in the stainless steel alloys immersed in the pure carbonate melt at 500°C. —◇— R_{corr} —○— σ.

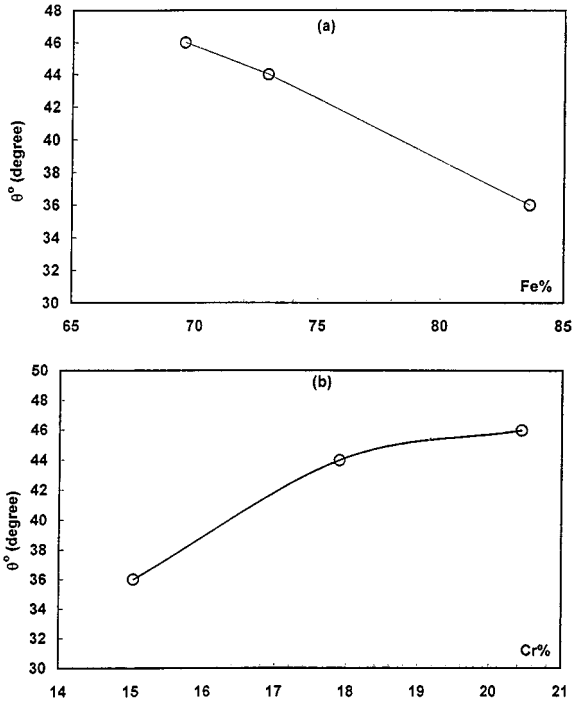

Figure 11 Variation of phase angle θ with Fe% (a) and Cr% (b) in the stainless steel alloys immersed in pure carbonate melt at 500°C.

While Fig. 11a and b represent the plots of phase angle (θ) versus Fe% and Cr% of the alloys. The results of table (3) and of Fig. 10a and b are in good agreement with those previously obtained by open circuit potential measurements.

3.4. Corrosion tests on the oxide scales

In this series of experiments trails are made to evaluate the corrosion resistance of the oxide scales formed on

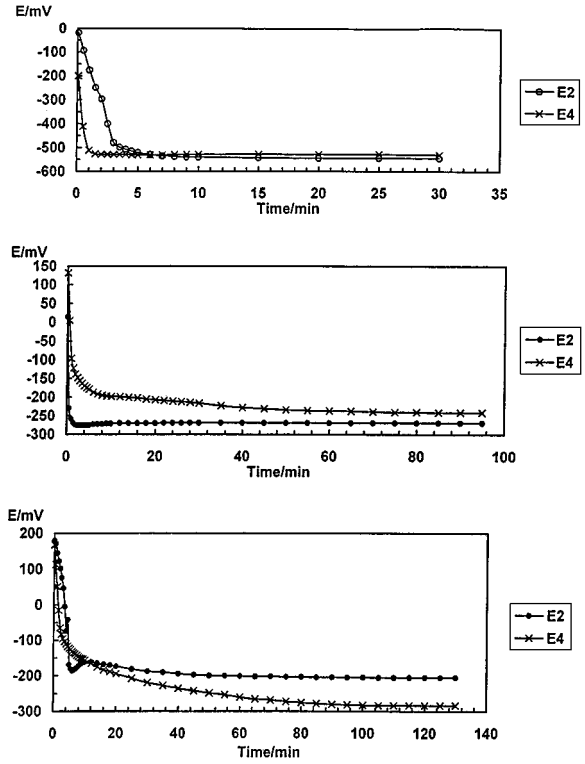

Figure 12 (a): Potential time curves for the stainless steel alloy 1 in 0.2 M HCl after oxidation in pure carbonate melt, under open circuit condition. $E2$, 500°C, $E4$, 550°C. (b): Potential time curves for the stainless steel alloy 2 in 0.2 M HCl after oxidation in pure carbonate melt under open circuit conditions. $E2$, 500°C, $E4$, 550°C. (c): Potential time curves for the stainless steel alloy 3 in 0.2 M HCl after oxidation in pure carbonate melt under open circuit condition. $E2$, 500°C. $E4$, 550°C.

the surface of the three stainless steel alloys after their immersion in carbonate melt. In these experiments, the preoxidized electrodes were immersed in 0.2 M HCl solution and their potential, measured against saturated calomel electrode, was followed as a function of time till reaching steady state, under the open circuit conditions at ambient temperature (around 22°C).

Fig. 12a–c represent, respectively, the potential-time curves for the three stainless steel alloys (1, 2, 3), immersed in 0.2 M HCl solution after their oxidation under open circuit conditions in pure carbonate melt at temperatures of 500 and 550°C. It is clear that, on immersion of the preoxidized electrodes in HCl solution, their potential greatly and then slowly shifts to more negative direction till attaining the steady state. The time required to reach this steady state, t_s, depends on the temperature of oxidation and the type of stainless steel alloy.

If we roughly consider the immersion potential, E_{imm} as the starting potential of the preoxidized electrode and the steady state potential, E_s, as the end potential, the value of dissolution potential range ($E_{imm} - E_s$) can be calculated. The time required for the shift of potential from E_{imm} to E_s, (time of dissolution) was recorded, t_s,. The rate of dissolution of oxide scales can be roughly calculated by dividing the value of dissolution potential range, ($E_{imm} - E_s$) by the time of dissolution t_s,. The obtained values of these calculations are listed in Table IV. Taking in consideration the undertest stainless steel alloys and the values of their

TABLE IV Data of the corrosion tests on the oxide scales of the stainless steel alloys

Alloy	Temp. (°C)	E_{imm} (mV)	E_s (mV)	$E_{imm} - E_s$ (mV)	t_s (min)	rate (mV/min)
No. 1	500	−18	−544	536	15	35.73
	500	−200	−530	330	3	110
No. 2	500	15	−269	284	24	11.83
	550	132	−240	372	75	4.96
No. 3	500	180	−205	385	105	3.67
	550	168	−283	451	100	4.51

rates of dissolution, we can conclude that the oxide scales formed on the surface of the austenitic stainless steel alloys (2, 3) are more resistance to dissolution than those formed on the ferritic stainless steel alloy (1). The values of E_{imm} for austenitic electrodes (2, 3) are more positive than that of the ferritic electrode, indicating that the oxide scales of the austenitic alloys are more passive than those of ferritic alloys. The values of E_s for austenitic electrodes are more positive than that for the ferritic electrode. This indicates that the oxide scales of the austenitic alloys are more resistant to dissolution in HCl acid solution than those of the ferritic alloy. Also, it seems that the oxide scales of austenitic alloys are multilayered. The outer layer of these scales is less protective and tends to dissolve in the acid, while the inner layer od scales has high resistance to dissolution in the present concentration of the acid solution.

Nomenclature

E_{imm}: Immersion potential
E_s: Steady state potential.
t_s: Time needed to reach steady state values.
k_f: Rate of formation of oxide scale
k_{-f}: Rate of dissolution of oxide scale
i_{Imm}: Immersion galvanic current
i_s: Steady state current.

References

1. J. M. KING, JR., Final Report, NASA CR, 134599, FCR-0237 (1977).
2. Quarterly Status Report for period Jan. 1–March 31, 1977, contract. No.31-109-38-3952, Institute of Gas technology, Chicago, I11.
3. R. B. SWAROOP, J. W. SIM and K. KINOSHITA, *J. Electrochem. Soc.* **125**(11) (1978) 1799.
4. R. A. DONADO, L. G. MARIANOWSKI, H. C. MARU and J. R. SELMAN, *ibid.* **131**(11) (1984) 2535.
5. *Idem., ibid.* **131**(11) (1984) 2541.
6. O. P. PENYAGINA, I. N. OZERYANAYA, N. D. SHAMANOVA and B. B. ANTONOV, *Tr. Inst. Electrochim., Ural Nauchn. Tsetr, Akad. Nauk SSSR* **26** (1978) 48.
7. R. T. COYLE, T. M. THOMAS and G. Y. LAI, in High Temp. Corros. Energy Syst. Proc. Symp. 672, 1984, edited by M. F. Rothman (Metall. Soc. AIME. Werrendal, PA 1985).
8. K. NAKAGAWA, T. ISOZAKI, S. KIHARA and B. GIJUSTU, **36**(7) (1987) 438.
9. H. KIYOSHI, Y. TAKATOSHI, Y. TAKEHIKO, F. YUTAKA and O. KEIZOU, *Zairyo to Kankyo* **40**(2) (1991) 130.
10. N. TATSUO, Y. KOHICHI and U. ISAMU, in Proc. Electrochem. Soc. 1993, 93 (Proceedings of the Third International Symposium on Carbonate Fuel Cell Technology, 1993, p. 264).
11. H. YOKOKAWA, N. SAKAI, T. KAWADA and M. DOKIYA, *J. Electrochem. Soc.* **140**(12) (1993) 3565.
12. J. P. T. VOSSEN, L. PLOMP, J. H. W. DE WIT and G. RIETVELD, *ibid.* **142**(10) (1995) 3327.
13. C. G. LEE, H. NAKANO, T. NISHINA, I. UCHIDA and S. KUROE, *ibid.* **145**(8) (1998) 2747.
14. S. SENDROFF and A. BRENNER, *ibid.* **101** (1954) 31.
15. J. O. M. BCKRIS, G. J. HILLS, D. INMAN and L. YOUNG, *J. Sci. Inster*. **33** (1956) 438.
16. S. N. FLENGAS and E. K. RIDEAL, *Proc. Roy. Soc*. **A233** (1956) 443.
17. S. N. FLENGAS and T. R. INGRAHAM, *Canad. J. Chem*. **35** (1957) 1139.
18. J. P. T. VOSSEN, A. H. H. JANSSEN and J. H. W. DE WIT. *J. Electrochem. Soc*. **143**(1) (1996) 58.
19. J. P. T. VOSSEN, R. C. MAKKUS and J. H. W. DE WIT, *ibid.* **143**(1) (1996) 66.
20. M. D. INGRAM, B. BARON and J. JANZ, *Electrochim. Acta* **11** (1966) 1629.
21. L. YOUNG, "Anodic Oxidation Films" (Academic Press, London, New York, 1961) p. 11257.
22. Z. SZLARSKA-SMIALOWSKA and R. W. STEEHLE, *J. Electrochem. Soc*. **12** (1974) 1393.
23. A. M. BEKHEET, M. M. HEFNY, A. A. MAZHAR and M. S. EL-BASIOUNY, *Ann. Chem. (Rome)* **73** (1983) 63.
24. M. S. EL-BASIOUNY, A. M. EL-KOT and M. M. HEFNY, *Corrosion* **36** (1980) 244.
25. U. R. EVANS "The Corrosion and Oxidation of Metals" (Edward Arnold, London, England, 1960) p. 898.
26. T. BUNZO and O. TAKEO, *Hyomen Gijutu* **43**(3) (1992) 233.
27. Q. W. WALTER, *Corros. Sc*. **26**(9) (1986) 681.
28. M. AZZI and J. J. RAMEAU, *ibid.* **30** (1990) 439.
29. J. P. T. VOSSEN, P. C. H. AMENT and J. H. W. DE WIT, *J. Electrochem. Soc*. **143**(7) (1996) 2272.

Received 12 November 1999
and accepted 3 August 2000